

# Coupling carbon nanotube mechanics to a superconducting circuit

B.H. Schneider<sup>1</sup>, S. Etaki<sup>1</sup>, H.S.J. van der Zant<sup>1</sup>, G.A. Steele<sup>1</sup>

<sup>1</sup>*Kavli Institute of NanoScience, Delft University of Technology, PO Box 5046, 2600 GA, Delft, The Netherlands.*

**The quantum behaviour of mechanical resonators is a new and emerging field driven by recent experiments reaching the quantum ground state. The high frequency, small mass, and large quality-factor of carbon nanotube resonators make them attractive for quantum nanomechanical applications. A common element in experiments achieving the resonator ground state is a second quantum system, such as coherent photons or superconducting device, coupled to the resonators motion. For nanotubes, however, this is a challenge due to their small size. Here, we couple a carbon nanoelectromechanical (NEMS) device to a superconducting circuit. Suspended carbon nanotubes act as both superconducting junctions and moving elements in a Superconducting Quantum Interference Device (SQUID). We observe a strong modulation of the flux through the SQUID from displacements of the nanotube. Incorporating this SQUID into superconducting resonators and qubits should enable the detection and manipulation of nanotube mechanical quantum states at the single-phonon level.**

The remarkable properties of nanoelectromechanical systems (NEMS) are useful for a wide variety of applications, such as ultra-sensitive force detection [1, 2, 3], mass detection at the single atom level [4, 5], and exploring the quantum limit of mechanical motion [6, 7, 8, 9, 10]. For all of these applications, sensitive detection of the resonator motion is crucial. The ultimate limit of the detection of the motion of a mechanical resonator is given by its quantum zero point fluctuations, which result in an uncertainty in the resonators position determined by the standard quantum limit[11].

An effective way of detecting the quantum motion of mechanical devices is to couple their displacement to another “probe” quantum system which can be read out and controlled, such as coherent quantum states of a superconducting qubit [8], coherent photons in a cold microwave resonator circuit [9], or the coherent fields of a laser [10]. In the last decade, superconducting circuits have emerged as an established platform for engineering and controlling quantum behaviour [12]. This has formed the motivation for many works coupling MEMS and NEMS devices to superconducting circuits [13, 2, 11, 14, 15, 8, 9]. By coupling microelectromechanical (MEMS) devices to quantum superconducting circuits, researchers have recently demonstrated mechanical resonators in their quantum ground state [8, 9] and achieved single-phonon control over their motion [8]. An outstanding challenge in these experiments is simultaneously achieving both a strong coupling at the single-phonon level, together with a high frequency and large quality factor for the mechanical resonator.

Carbon nanotube mechanical resonators [16, 17, 18] possess a unique combination of large quality factor, small mass, and high frequency. Because of their small size, however, it is not easy to couple to their quantum motion. Techniques based on a capacitive interaction with superconducting qubits or microwave photon cavities, as was done in recent experiments with MEMS devices reaching the mechanical quantum ground state [8, 9], do not provide sufficient coupling strength. An alternative is to incorporate the mechanical element into a SQUID, as was demonstrated recently using micromechanical beams [19]. If a carbon nanotube NEMS element could be included in a SQUID, the SQUID could then be used as a transducer to couple the mechanical motion to a superconducting cavity [20], or as the basis for a superconducting qubit, coupling the motion directly to the quantum states of the qubit.

Here, we demonstrate the coupling of a carbon nanotube NEMS device to a superconducting circuit, based on a suspended carbon nanotube SQUID. The flux through the SQUID couples to the nanotube

arXiv:1209.1514v1 [cond-mat.mes-hall] 7 Sep 2012

displacement with a strength of  $0.36 \text{ m}\Phi_0/\text{pm}$ . This new device opens up the possibility of combining carbon NEMS devices with the quantum toolkit from the superconducting community. Doing so, we expect the suspended nanotube SQUID will provide a platform for detection of the nanotube resonator's ground state, and control over its motion at the level of single phonons.

## Results

The device consists of a SQUID in which the two Superconductor-Normal metal-Superconductor (SNS) weak links are made from carbon nanotube junctions [21, 22, 23]. In contrast to earlier works, the carbon nanotubes are freely suspended, and thus also act as NEMS elements embedded in the SQUID. To make the suspended nanotube SQUID, a clean carbon nanotube is grown in the last step of fabrication [24] over a trench patterned between metal source and drain contacts made from a MoRe superconducting alloy (see Methods). A Scanning Electron Microscope (SEM) image of a typical device is shown in Fig. 1a. The doped substrate below the trench is used as a global backgate. The device is mounted in a superconducting magnet coil with the magnetic field aligned in the plane of the sample, parallel to the trenches, as indicated in Fig. 1b. The magnetic field orientation is chosen to maximize the coupling of vertical displacements on the nanotube to flux in the SQUID loop [19]. A small misalignment of the sample also induces a magnetic field perpendicular to the sample surface which is used to tune the flux operating point of the SQUID.

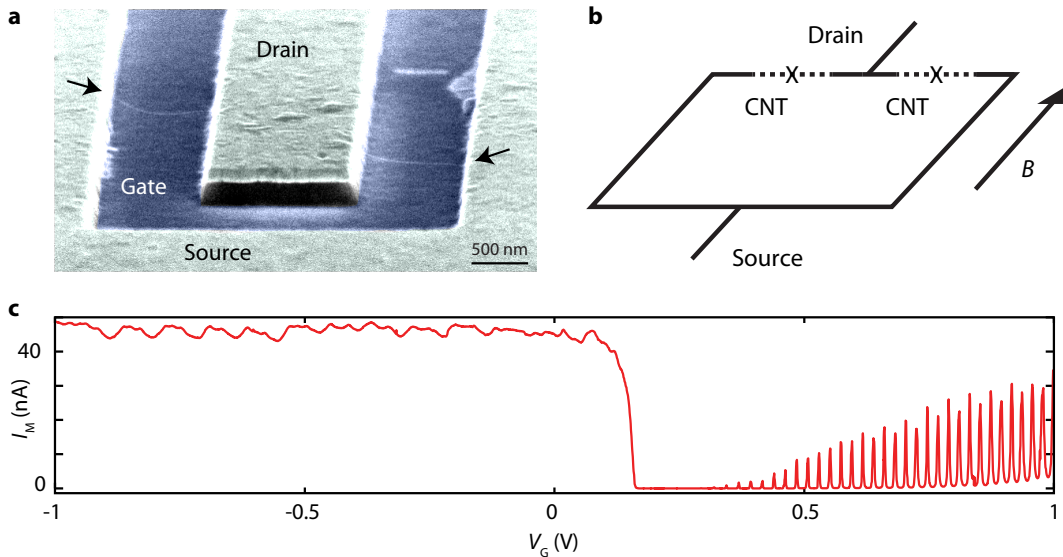


**Figure 1: Design and characterization of the device** **a**, Colorised scanning electron microscope (SEM) image of a typical device showing a single carbon nanotube (CNT) crossing two trenches. The device is made by etching two 800 nm wide trenches in a MoRe layer and underlying  $\text{SiO}_2$ , and subsequently growing CNTs over the prefabricated structure. We apply a voltage  $V_G$  to the doped substrate underneath the  $\text{SiO}_2$ , which acts as a gate. **b**, Schematic drawing of the SQUID. The two suspended segments of the CNT form two SNS-type Josephson junctions, indicated by the crosses. An external magnetic field  $B$  can be applied in-plane along the trench. **c**,  $I_M$  as a function of  $V_G$  measured with an applied source-drain bias voltage  $V_B = 2 \text{ mV}$ . For  $V_G > 0.3 \text{ V}$ , the suspended segments form a p-n-p quantum dots exhibiting Coulomb blockade. For  $V_G < 0.2 \text{ V}$ , the CNT is doped with holes, showing Fabry-Perot oscillations with high conductance.

Figure 1c shows the current through the device ( $I_M$ ) as a function of the applied gate voltage ( $V_G$ ). From the gate voltage thresholds for electron and hole conduction, we estimate that the carbon nanotube

has a small bandgap of 40 meV (see Supplementary Information). Due to a work function difference present between the nanotube and the metal contacts, the nanotube is doped with holes near the edge of the trench. At positive gate voltages, electrons induced by the gate are confined by p-n junction tunnel barriers [24] in a Coulomb-blockaded quantum dot. For negative gate voltages, holes are induced in the suspended segment with no tunnel barriers. Here, instead of Coulomb blockade, conductance oscillations arising from Fabry-Perot electronic interference [25] are observed with conductances of up to  $4.7 e^2/h$  (see Fig. 2a). Note that this value exceeds the maximum conductance expected for a single carbon nanotube ( $G_{\max} = 4 e^2/h$ ), consistent with a SQUID geometry (Fig. 1b) where there are two carbon nanotube junctions in parallel (Fig. 1a).

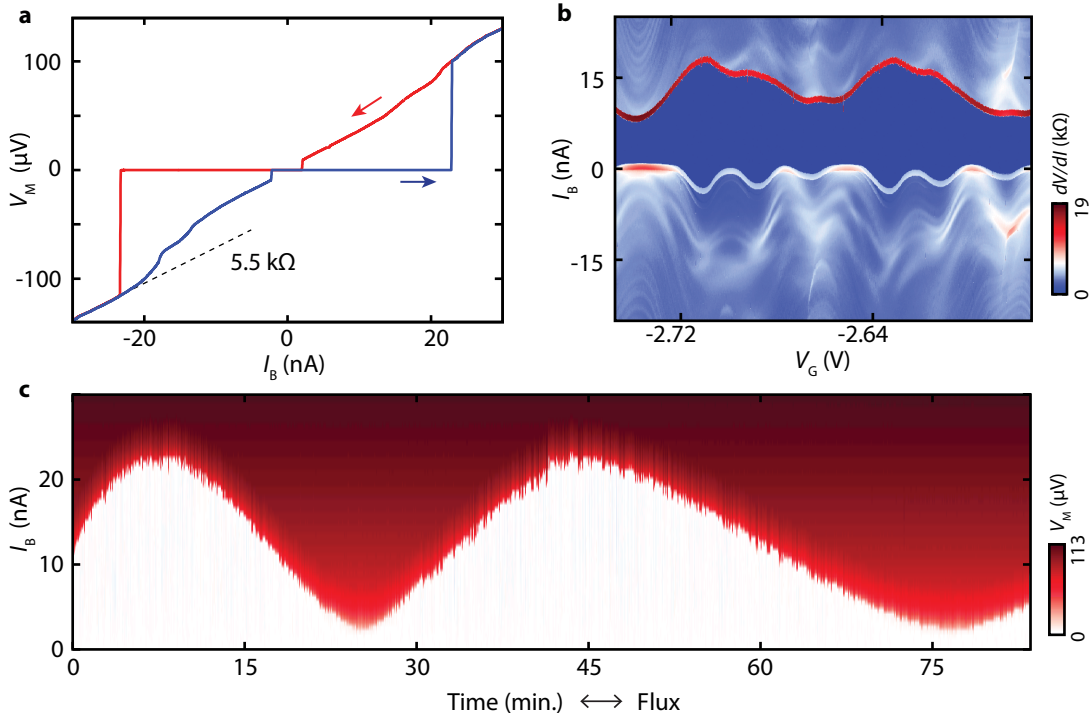


**Figure 2: A suspended carbon nanotube SQUID** **a**, Four-terminal current-voltage trace at  $V_G = -1.1$  V. The onset of the resistive branch occurs at 24 nA, corresponding to a critical current of 12 nA per nanotube junction. The dashed line indicates the normal-state resistance of 5.5 kOhm ( $G = 4.7 e^2/h$ ). The device is hysteretic, as can be seen from the forward (blue) and reverse (red) sweep directions [26]. **b**, Differential resistance  $dV_M/dI_B$  (color map) as a function of  $I_B$  and  $V_G$  (forward sweep direction). The critical current (red stripe at positive  $I_B$ ) oscillates with  $V_G$ , following the modulation of the normal state conductance. **c**, SQUID voltage  $V_M$  as a function of applied current  $I_B$  and time, taken at  $B = 0$  and  $V_G = -1.1$  V. Flux creep in the superconducting magnet coil is used to apply a small time varying magnetic field. The critical current oscillates from 2 nA up to 24 nA as a function of the flux through the SQUID. The near complete suppression of  $I_C$  at the minima indicates that the SQUID has highly symmetric junctions.

In Fig. 2, we use the gate to dope the nanotube with holes such that the device is tuned into the high-conductance Fabry-Perot regime, and measure the voltage across the SQUID as a function of an applied bias current (Fig. 2a). At low currents, the voltage across the device is zero, a clear indication of a proximity effect induced supercurrent. At a critical current of 24 nA, there is a switch to a finite voltage state. We attribute the large critical current in our junctions (12 nA per nanotube) to the high

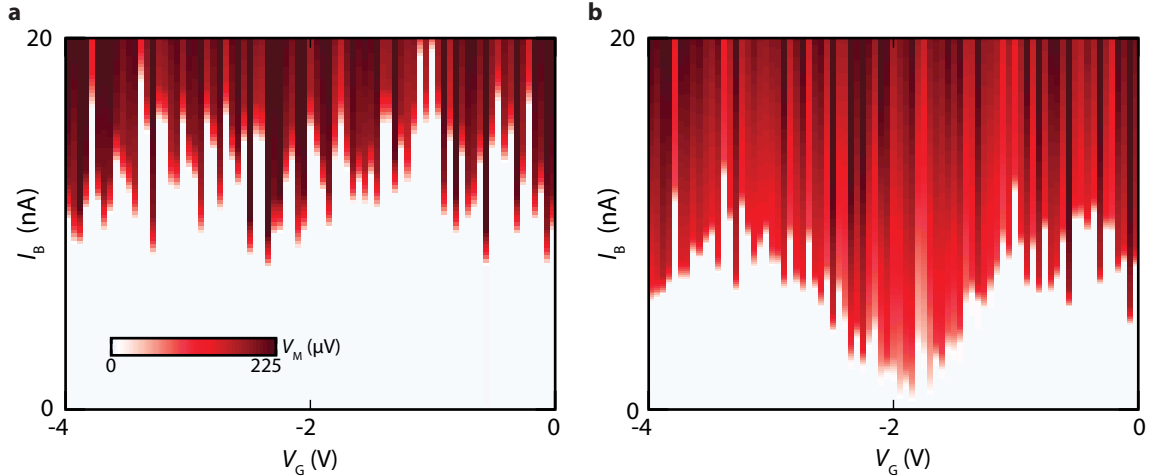


**Figure 3: A gate-voltage induced magnetic flux** **a**, Colormap of  $V_M$  as a function of  $I_B$  and  $V_G$ , taken at  $B = 0$  T. The critical current  $I_C$  is defined by the onset of a finite voltage state, indicated by the red regions. The Fabry-Perot modulation of the critical current (Fig. 2b) is visible as rapid fluctuations in  $I_C$  due to the large steps in  $V_G$ . The measurement is performed fast enough such that the magnetic field creep (Fig. 2c) can be neglected. **b**, Same measurement taken at  $B = 250$  mT. An additional approximately sinusoidal modulation of the critical current is seen with a gate periodicity of  $\Delta V_G = 2.5$  V.

critical temperature of the superconducting metal leads ( $T_C = 5.5$  K), the low contact resistance between the superconducting metal and the nanotube, and the clean electronic characteristics of the carbon nanotube. As shown in Fig. 2b, the critical current is strongly modulated by the gate through to gate dependence of the normal-state conductance [21]. Due to the high transparency of the superconductor-nanotube interface, the supercurrent in our device also remains finite in the valleys between the peaks in conductance.

To demonstrate that the device acts as a SQUID, we measure the critical current as a function of the flux through the loop. In practice, we do this by sweeping a large in-plane magnetic field to zero and then subsequently measure the critical current as a function of time. Due to creep in the superconducting magnet coil and the slight misalignment of the field to the sample plane, there is a small magnetic field component perpendicular to the surface that continues to change slowly after the sweep is completed. In such a measurement, shown in Fig. 2c, the observed critical current oscillates between a value of 24 nA and 2 nA. These oscillations result from quantum interference of the superconducting wavefunction traversing the two junctions of the SQUID [26]. The large sensitivity of the critical current to the flux from the small magnetic field creep, together with the single periodicity, is consistent with a single large SQUID loop formed by one nanotube SNS junction across each trench, as shown in the SEM image of a typical device in Fig. 1a.

We now turn our attention to the behaviour of the device in the presence of a static in-plane magnetic field applied parallel to the trench. Figures 3a and 3b show the gate voltage dependence of the critical current with and without an external magnetic field. The measurements are taken intentionally with a coarse gate voltage resolution such that the measurement time is short compared to the timescale of the flux creep (see Supplementary Information for further details). The steps in gate voltage are much larger than the periodicity of the Fabry-Perot conductance oscillations (Fig. 2a); consequently, these appear in Fig. 3a as (reproducible) single-pixel fluctuations. Figure 3b shows the same measurement taken at an external magnetic field of 250 mT. Here, an additional nearly sinusoidal modulation of the critical current

can be seen as a function of gate voltage with a periodicity much longer than that of the Fabry-Perot conductance oscillations.

In the following, we show how this additional gate modulation of the critical current arises from a change in magnetic flux induced by the d.c. gate voltage. The mechanism for such a gate induced flux is illustrated in Fig. 4b. Increasing the gate voltage, the nanotube is pulled towards the gate by the attractive electrostatic force between them. The nanotube displacement introduces an extra area  $\Delta A$  of the SQUID loop perpendicular to the magnetic field aligned along the trench. This area change results in a flux change linearly proportional to the displacement,  $\Delta\Phi \propto B\ell u$ , where  $B$  is the in-plane magnetic field,  $\ell$  is the nanotube length, and  $u$  is the vertical displacement of the nanotube. If the displacement  $u$  is linear in the gate voltage (as expected for certain gate voltage ranges, see Supplementary Information for further discussion), the critical current of the SQUID will then oscillate as a function of gate voltage with constant periodicity, as observed in Fig. 3b.

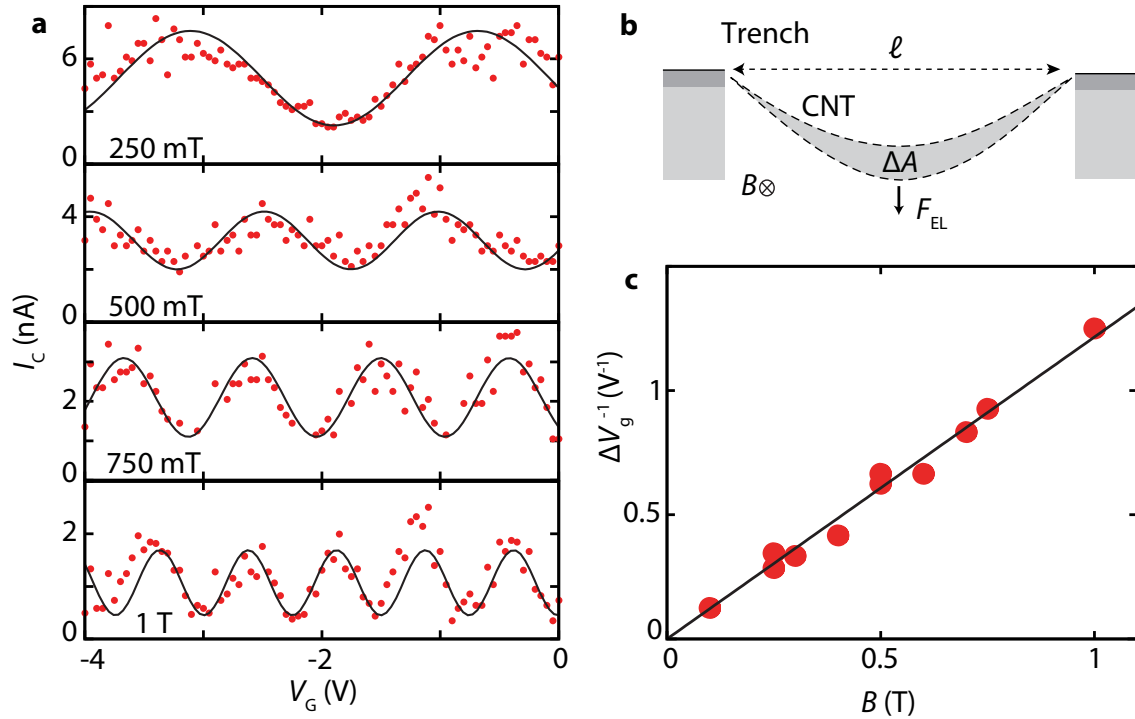


**Figure 4: Mechanical flux coupling** **a**, Extracted  $I_C$  (dots) as a function of  $V_G$  at four different magnetic fields. Lines show a sinusoidal fit to the data (red points) from which the periodicity  $\Delta V_G^{-1}$  is extracted. At  $B = 1$  T, five oscillations are visible corresponding to a flux change of  $5 \Phi_0$ . **b**, Vertical displacement of the nanotube due to the electrostatic force from the gate changes the area of the SQUID loop perpendicular to the in-plane magnetic field. This produces a gate-induced flux change proportional to the nanotube displacement, resulting in an  $I_C$  that oscillates with  $V_G$ . We estimate that the nanotube displaces by 7.4 nm as  $V_G$  is swept from 0 to -4 V ( $\Delta A \sim 5.5 \times 10^{-3} \mu\text{m}^2$  per nanotube). **c**,  $\Delta V_G^{-1}$  (dots) as a function of magnetic field with a linear fit (black line). At  $B = 1$  T, the flux couples to the vertical displacement of the nanotube with a flux coupling of  $0.36 \text{ m}\Phi_0/\text{pm}$ .

If this gate-voltage induced flux indeed arises from a mechanical displacement of the nanotube, the flux coupling should scale linearly with the external magnetic field. Figure 4a shows the extracted  $I_C$  versus  $V_G$  for fields up to 1 T. To extract the gate periodicity of the flux oscillation, the critical current as a function of gate voltage is fit to a sinusoidal function in order to approximate the expected oscillatory

SQUID response [26]. The resulting gate frequency  $V_G^{-1}$  is plotted as a function of magnetic field in Fig. 4c. The linear scaling of the periodicity with magnetic field demonstrates that the modulation is due to a flux originating from the mechanical displacement of the nanotube. At magnetic fields of 1 T, we couple the motion of the nanotube to the flux in the SQUID with a coupling strength of  $0.36 \text{ m}\Phi_0/\text{pm}$  (see Supplementary Information).

## Discussion

In the previous section, we demonstrate a strong coupling of the flux in a SQUID to the displacement of the carbon nanotube NEMS device. The strong flux coupling is, on its own, not unique to our device: for example, a larger mechanical flux responsivity was observed in a top-down fabricated SQUID [19]. What is unique to our device is the combination of such a flux coupling with a mechanical resonator with small mass (attogram) and large zero point fluctuations. This can be quantified in terms of the amount of flux noise the mechanical zero-point fluctuations would induce in the SQUID. The expected zero point motion of the nanotube is on the order of  $u_{\text{ZPF}} = \sqrt{\hbar/2m\omega} = 3.6 \text{ pm}$ . Together with a quality factor of  $3 \times 10^4$  and a mechanical resonance frequency of 125 MHz observed in this device (see Supplementary Information), this results in a peak in the flux noise spectrum of the SQUID at the mechanical resonance frequency with an amplitude of  $16 \mu\Phi_0/\sqrt{\text{Hz}}$ . This noise level, corresponding to the imprecision noise from the standard quantum limit for our device, is nearly two orders of magnitude larger than the  $0.2 \mu\Phi_0/\sqrt{\text{Hz}}$  sensitivity that has been demonstrated coupling a SQUID to a superconducting resonator [27]. Doing so, we expect that such a high frequency suspended carbon nanotube SQUID can be used as a linear position detector with an imprecision noise below the standard quantum limit, enabling the detection of the quantum motion of a carbon nanotube.

Finally, the strong coupling between flux and nanotube displacement could also be used to implement a nanomechanical resonator coupled to a superconducting qubit. The important characterization of the coupling between the two quantum systems is the zero-phonon coupling rate  $g$ , given by the energy shift of the probe quantum system in response to the zero-point fluctuations of the mechanical device [10]. In order to have a coherent interaction between the probe and the mechanical system at the single-phonon level, the coupling rate  $g$  must be larger than the decoherence rates of quantum states of the mechanical system and probe system. Incorporating a nanotube SQUID into a transmon-qubit design would achieve a single-phonon coupling rate of  $g = 7 \text{ MHz}$  (see Supplementary Information). Such a coupling strength would be within the single-phonon strong-coupling limit, providing a means for the readout and control of mechanical quantum states of a carbon nanotube.

## Methods

Fabrication begins with an oxidized p++ Si wafer (285 nm oxide), in which the doped substrate is used as a global backgate. A 40/40 nm Mo/Re bilayer is deposited by magnetron sputtering, and electrodes are subsequently defined by reactive ion etching with an  $\text{SF}_6$  plasma. Reactive ion etching is continued into the substrate, also defining self-aligned trenches in the  $\text{SiO}_2$ . The Mo and Re in the two separate layers subsequently alloy together during the nanotube growth step. The resulting film is a superconductor with a  $T_C$  of 5.5 K. Nanotubes are grown over the structure in the last step using a methane CVD growth [24], and promising devices are selected from room-temperature electrical characterization. Measurements are performed in a dilution refrigerator at a base temperature of 25 mK. The device is connected via copper powder filters and low pass filters at base temperature to the measurement equipment at room temperature. Measurements are performed in either a 4-terminal current bias or a 2-terminal voltage bias configuration.

## References

- [1] Rugar, D., Budakian, R., Mamin, H. & Chui, B. Single spin detection by magnetic resonance force microscopy. *Nature* **430**, 329–332 (2004).
- [2] Regal, C., Teufel, J. & Lehnert, K. Measuring nanomechanical motion with a microwave cavity interferometer. *Nature Phys.* **4**, 555–560 (2008).
- [3] Usenko, O., Vinante, A., Wijts, G. & Oosterkamp, T. A superconducting quantum interference device based read-out of a subattoneutron force sensor operating at millikelvin temperatures. *Appl. Phys. Lett.* **98**, 133105 (2011).
- [4] Jensen, K., Kim, K. & Zettl, A. An atomic-resolution nanomechanical mass sensor. *Nature Nanotech.* **3**, 533–537 (2008).
- [5] Chaste, J. *et al.* A nanomechanical mass sensor with yoctogram resolution. *Nature Nanotech.* **7**, 301–304 (2012).
- [6] Schwab, K. & Roukes, M. Putting mechanics into quantum mechanics. *Phys. Today* **58**, 36–42 (2005).
- [7] Poot, M. & van der Zant, H. Mechanical systems in the quantum regime. *Phys. Rep.* **511**, 273–335 (2012).
- [8] O’Connell, A. *et al.* Quantum ground state and single-phonon control of a mechanical resonator. *Nature* **464**, 697–703 (2010).
- [9] Teufel, J. *et al.* Sideband cooling of micromechanical motion to the quantum ground state. *Nature* **475**, 359–363 (2011).
- [10] Chan, J. *et al.* Laser cooling of a nanomechanical oscillator into its quantum ground state. *Nature* **478**, 89–92 (2011).
- [11] Teufel, J., Donner, T., Castellanos-Beltran, M., Harlow, J. & Lehnert, K. Nanomechanical motion measured with an imprecision below that at the standard quantum limit. *Nature Nanotech.* **4**, 820–823 (2009).
- [12] Clarke, J. & Wilhelm, F. Superconducting quantum bits. *Nature* **453**, 1031–1042 (2008).
- [13] Naik, A. *et al.* Cooling a nanomechanical resonator with quantum back-action. *Nature* **443**, 193–196 (2006).
- [14] Rocheleau, T. *et al.* Preparation and detection of a mechanical resonator near the ground state of motion. *Nature* **463**, 72–75 (2009).
- [15] LaHaye, M., Suh, J., Echternach, P., Schwab, K. & Roukes, M. Nanomechanical measurements of a superconducting qubit. *Nature* **459**, 960–964 (2009).
- [16] Sazonova, V. *et al.* A tunable carbon nanotube electromechanical oscillator. *Nature* **431**, 284–287 (2004).
- [17] García-Sánchez, D. *et al.* Mechanical detection of carbon nanotube resonator vibrations. *Phys. Rev. Lett.* **99**, 85501 (2007).
- [18] Hüttel, A. *et al.* Carbon nanotubes as ultrahigh quality factor mechanical resonators. *Nano Lett.* **9**, 2547–2552 (2009).

- [19] Etaki, S. *et al.* Motion detection of a micromechanical resonator embedded in a dc SQUID. *Nature Phys.* **4**, 785–788 (2008).
- [20] Buks, E., Zaitsev, S., Segev, E., Abdo, B. & Blencowe, M. Displacement detection with a vibrating rf superconducting interference device: Beating the standard linear limit. *Phys. Rev. E* **76**, 026217 (2007).
- [21] Jarillo-Herrero, P., Van Dam, J. & Kouwenhoven, L. Quantum supercurrent transistors in carbon nanotubes. *Nature* **439**, 953–956 (2006).
- [22] Cleuziou, J., Wernsdorfer, W., Bouchiat, V., Ondarçuhu, T. & Monthieux, M. Carbon nanotube superconducting quantum interference device. *Nature Nanotech.* **1**, 53–59 (2006).
- [23] Liu, G., Zhang, Y. & Lau, C. Gate-tunable dissipation and “superconductor-insulator” transition in carbon nanotube Josephson junctions. *Phys. Rev. Lett.* **102**, 16803 (2009).
- [24] Steele, G., Gotz, G. & Kouwenhoven, L. Tunable few-electron double quantum dots and Klein tunnelling in ultraclean carbon nanotubes. *Nature Nanotech.* **4**, 363–367 (2009).
- [25] Liang, W. *et al.* Fabry-perot interference in a nanotube electron waveguide. *Nature* **411**, 665–669 (2001).
- [26] Clarke, J. & Braginski, A. *The SQUID handbook*, vol. 1 (Wiley Online Library, 2006).
- [27] Hatridge, M., Vijay, R., Slichter, D., Clarke, J. & Siddiqi, I. Dispersive magnetometry with a quantum limited SQUID parametric amplifier. *Phys. Rev. B* **83**, 134501 (2011).

## Acknowledgments

This work was supported by the Dutch Organization for Fundamental Research on Matter (FOM), the Netherlands Organization for Scientific Research (NWO), and the EU FP7 STREP program (QNEMS).

## Author Contributions

B.H.S. fabricated the sample. B.H.S. and S.E. conducted the experiments. B.H.S. and G.A.S. wrote the manuscript. G.A.S. and H.v.d.Z. supervised the project. All authors discussed the results, analyzed the data, and commented on the manuscript.



# Coupling carbon nanotube mechanics to a superconducting circuit: Supplementary Information

B.H. Schneider<sup>1</sup>, S. Etaki<sup>1</sup>, H.S.J. van der Zant<sup>1</sup>, G.A. Steele<sup>1</sup>

<sup>1</sup>*Kavli Institute of NanoScience, Delft University of Technology, PO Box 5046, 2600 GA, Delft, The Netherlands.*

## S1 Device characterization

In Fig. S1, we present electrical measurements characterizing the transport properties of the device, in which the Coulomb blockade and Fabry-Perot transport regimes for different gate voltages can be seen, and from which the bandgap is estimated.

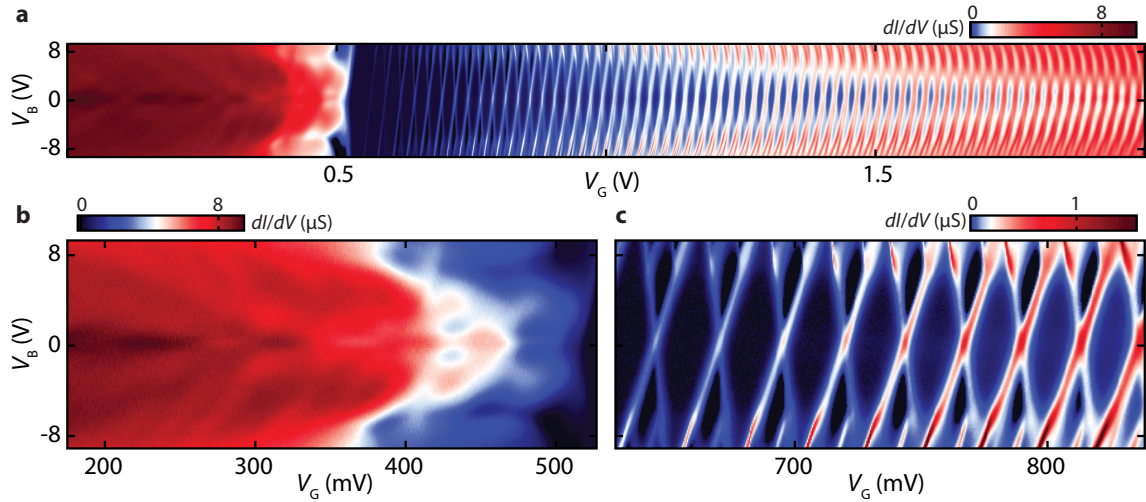


**Figure S1:** Two-terminal differential conductance **a**, as a function of the source-drain bias voltage  $V_B$  and gate voltage  $V_G$ , taken at 1.2 K (series resistance from wiring and filters has not been subtracted). This dataset was taken during an earlier cooldown of the device in a different cryogenic insert. As a result, there is a slight shift of the threshold gate voltage for hole conductance compared to Fig. 1c of the main text. We determine the bandgap of the device from the size of the empty Coulomb diamond by subtracting the average of the  $1e/1h$  addition energies from the empty-dot addition energy. **b**, Zoom of the dataset showing the high-conductance Fabry-Perot regime when doping the device with holes. **c**, Zoom of dataset showing Coulomb blockade when the device is doped with electrons. When doping the device with electrons, tunnel barriers naturally form from p-n junctions near the edge of the trench. The p-n junctions arise from a gate-independent p-type doping of the nanotube near the trench edge due to the work function difference between the nanotube and the metal contacts.

## S2 Discriminating gate-induced flux from time-dependent flux creep

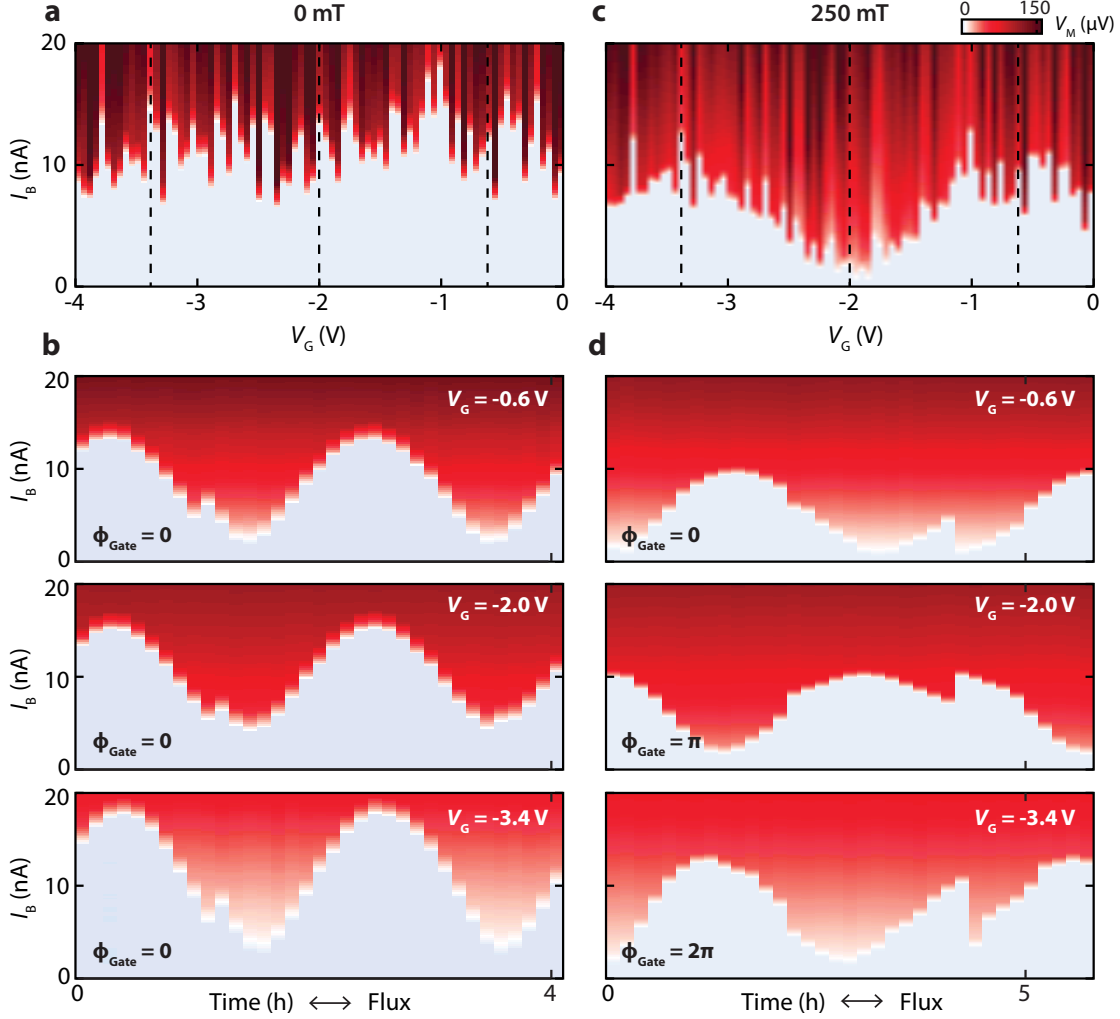


**Figure S2: Gate-voltage induced flux observed by a gate-dependent shift of the phase of the time-dependent oscillations of  $I_C$**  **a**, Voltage  $V_M$  as a function of applied bias current  $I_B$  and gate voltage  $V_G$  at  $B = 0$ . **b**,  $V_M$  as a function of  $I_B$  and of time for three different gate voltages indicated by the dashed in **a**. **c,d** Same measurement as in **a,b**, but now taken in the presence of a parallel magnetic field of 250 mT. **d**, A gate dependent phase shift  $\Phi_{Gate}$  of the oscillations of  $I_C$  is now observed, demonstrating that the gate voltage is inducing a magnetic flux in the SQUID.

In this section, we present measurements which discriminate between time dependent magnetic flux creep (Fig. 2c in the main text) and gate-induced flux (Fig. 3b of the main text). This is done by plotting the time-dependent oscillations of  $I_C$  at different gate voltages. If the gate is inducing no flux in the SQUID, the oscillations at different gate voltages should all be in phase. If the gate is inducing a flux in the SQUID, there will be a phase shift between the oscillations at different gate voltages.

In Fig. S2, we demonstrate that at  $B = 0$ , the oscillations in time at different gate voltages are in phase, while  $B = 250$  mT, they are shifted by the gate-induced flux. The data in Fig. S2 are extracted from a 3-D  $(x, y, z) = (I_B, V_G, t)$  dataset (one at  $B = 0$  and one at  $B = 250$  mT). The measurements are performed by sweeping the bias current, stepping the gate voltage quickly, and then repeating this in

time. The gate sweep is performed quickly enough such that the measurement time for a full gate sweep measurement, as shown in Fig. S2a, is fast compared to the external flux drift: the measurement time for such a gate sweep is  $t_{meas} = 7$  min, while the external flux creep rate during these measurements is about  $1 \Phi_0$  in two hours. Each gate sweep can therefore be considered to be taken at a fixed external flux. Note that in addition to the slow flux creep, we also sometimes observe sudden jumps in the external flux, such as can be seen at  $t = 4.2$  hours in Fig. S2d. This results in a sudden jump in the phase of the oscillations. The gate induced phase shift, however, can still be tracked both immediately before and after the jump. The gate traces in Fig. S2 and Fig. 3 of the main text are extracted at timesteps where these flux jumps are not present.

Figure S2b shows  $I_C$  vs. time for three different gate voltages at  $B = 0$ . At zero external field, the oscillations of  $I_C$  measured at different gate voltages are all in phase, indicating no gate-induced flux. In Fig. S2d, we show  $I_C$  oscillations in time at  $B = 250$  mT. The d.c. gate voltage now shifts the phase of the oscillations, as can be seen clearly in Fig. S2d. This gate-dependent phase shift demonstrates that the gate-induced sinusoidal modulation of  $I_C$  shown in Fig. S2c, and Fig. 3c of the main text, are indeed caused by a gate-voltage induced magnetic flux.

### S3 Expected static displacement of the nanotube with gate voltage

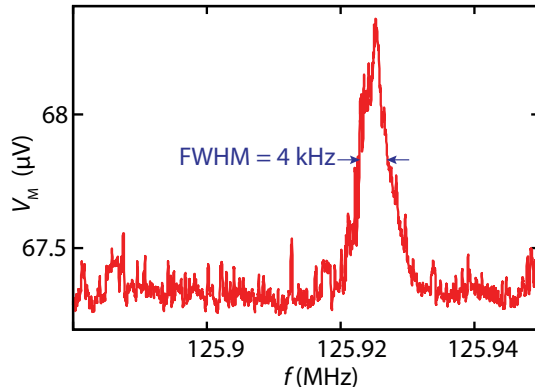


**Figure S3: Driven mechanical resonance of the nanotube** measured by applying a bias current above the critical current and using rectification readout technique introduced in [1]. We estimate the quality factor of the resonance from the full width at half maximum,  $\Delta f$ , of the measured curve. With  $f_R = 126$  MHz and  $\Delta f = 4$  kHz, we get  $Q = f_R/\Delta f = 3 \times 10^4$ .

When a constant voltage  $V_G$  is applied to the gate, the suspended nanotube segments are attracted to the gate by a Coulomb force,  $F_C \propto V_G^2$ . The equilibrium position of the nanotube corresponds to the position where this Coulomb force is balanced by the mechanical restoring force [2]. At small gate voltages, the bending rigidity of the nanotube dominates the mechanical restoring force, giving a static displacement  $u \propto V_G^2$  (the weak bending regime). Beyond a certain gate voltage, induced tension in the nanotube becomes important in determining the mechanical restoring force, and there is a transition to a strong bending regime in which  $u \propto V_G^{2/3}$ . The transition between these two regimes depends on the dimensions of the nanotube, and can also be influenced by additional tension introduced, for example, by the fabrication process. In any case, the net result is that the displacement of the nanotube as a function of gate voltage is, to a good approximation, linear over a relatively wide regime of voltages, as can be seen in Fig. 2 of Sapmaz *et al.* [2].

If the nanotube displacement was not linear in gate voltage, the periodicity of the  $I_C$  oscillations in gate voltage,  $\Delta V_G^{-1}$ , would change slowly as a function of gate voltage. The relatively constant  $\Delta V_G^{-1}$  we observe in Fig. 4a of the main text indicates that the nanotube displacement in our device is indeed approximately linear in the range of gate voltages we study.

Critical current oscillations in gate voltage were fitted to a cosine function:

$$f(x) = \frac{a+b}{2} + \frac{a-b}{2} \cos \left[ (x-x_0) \frac{2\pi}{L} \right] \quad (1)$$

where  $a$  and  $b$  are the maximum and minimum of the modulation respectively, and where  $x_0$  is the position at the maximum and  $L$  the periodicity.

## S4 Definition of the nanotube displacement and estimation of the flux responsivity

In this section, we give a rigorous definition of the nanotube displacement, and use this definition to calculate the flux responsivity of the device. In particular, following Poot *et al.* [3], we define the displacement of a mode of the nanotube in such a way that we require only one effective mass for all modes, avoiding the complication of having different effective masses for different modes.

The zero-frequency, or dc, flexural displacement  $z_{\text{dc}}(x, y)$  of the carbon nanotubes towards the back gate (the  $x-y$  plane), can be described by a single coordinate  $u_{\text{dc}}$ . The displacement per unit force and the change of area  $\Delta A$  per unit displacement both depend on the chosen definition of  $u_{\text{dc}}$ . This is also true for the mechanical resonance modes of the nanotube, which form an eigenbasis for the nanotube displacement. Any periodic displacement of the nanotube with frequency  $f$  can be decomposed into a superposition of the eigenmodes:

$$z(x, y, t) = \sum_0^{\infty} u_n \xi_n(x, y) \cos(2\pi f t + \varphi_n), \quad (2)$$

where  $u_n$  is the displacement coordinate,  $\xi_n(x, y)$  is the normalized mode shape,  $f_n$  is the eigenfrequency and  $\varphi_n$  is the phase offset of mode  $n$ . For a nanotube with length  $\ell$  much larger than its cross-sectional diameter,  $\xi_n(x, y)$  is usually integrated in the radial direction, such that the mode shape can be described as a function of only the distance along its length direction,  $x$ , i.e.  $\xi_n(x, y) \rightarrow \xi_n(x)$ . The dc displacement ( $f = 0$ ) is related to the eigenmodes by:

$$z_{\text{dc}}(x) = \sum_0^{\infty} u_n \xi_n(x). \quad (3)$$

In general, the displacement, modeshapes and eigenfrequencies of the nanotube must be solved from its elastodynamic differential equations and depend on the nanotube geometry, its rigidity, any built-in tension, and the amount and distribution of applied forces. Once this is done, the definition of displacement depends on the choice of normalization for  $\xi_n(x)$ . A convenient normalization for  $\xi_n(x)$  is:

$$\frac{1}{\ell} \int_0^{\ell} \xi_n(x)^2 dx = 1. \quad (4)$$

With this normalization, the displacement coordinate  $u_n$  is (spatial) root-mean-square displacement of mode  $n$ . The dynamical spring constant of each eigenmode now equals  $k_n = m_{\text{R}}(2\pi f_n)^2$ , where  $m_{\text{R}}$  is the nanotube mass. The change in area due to a d.c. nanotube displacement becomes:

$$\Delta A = \int_0^{\ell} z_{\text{dc}}(x) dx = \sum_0^{\infty} a_n \ell u_n, \quad (5)$$

$$a_n \equiv \frac{1}{\ell} \int_0^{\ell} \xi_n(x) dx. \quad (6)$$

To estimate the numerical coefficients  $a_n$ , we assume sinusoidal eigenmode shapes for the nanotubes:  $\xi_n(x) = \sqrt{2} \sin(\pi n x / \ell)$  (based on [3]). The numerical coefficients then become  $a_n = 0.9/n$  for odd  $n$  and  $a_n = 0$  for even  $n$  (no net area change). For a displacement due to a uniformly distributed dc force, the amplitude of each eigenmode is proportional to  $(a_n/f_n)^2$ , which means that the shape of the dc deflection is almost entirely determined by the fundamental eigenmode ( $f_n$  is roughly proportional to  $n$ ). The dc spring constant is then equal to  $k_1$  and the area change for both  $u_{dc}$  and  $u_1$  is characterized by the same coefficient,  $a_1 = 0.9$ .

Having defined the displacement, we are now in a position to calculate the responsivity of the device. The flux responsivity  $\Phi_u$  which we give in the main text is calculated by multiplying  $\Delta A$  with the applied magnetic field  $B$  and dividing out the displacement  $u_{dc}$ :

$$\Phi_u \equiv \frac{d\Phi}{du_{dc}} \approx \frac{d\Phi}{du_1} = a_1 B \ell. \quad (7)$$

At a field of 1 T and a suspended nanotube length of 800 nm, we get a responsivity  $\Phi_u = 0.35 \Phi_0/\text{nm}$  per suspended nanotube segment. The dc displacement of the nanotube due to the applied gate voltage can now be calculated based on Fig. 4a of the main text: At 1 T, we observe five oscillations of the SQUID critical current, i.e.  $\Delta\Phi = 5\Phi_0$ . With the calculated responsivity, the displacement of each nanotube segment over the full gate voltage range is  $\Delta\Phi/\Phi_u = 7$  nm.

## S4 Estimation of the zero point motion

Quantum mechanical displacement fluctuations are dominant when a mechanical resonator with resonance frequency  $f_R$  is cooled to a temperature  $T$  such that its thermal energy is far less than the energy of a single phonon, i.e.  $k_B T \ll h f_R$ . Here,  $k_B$  is the Boltzmann constant and  $h$  is the Planck constant. In this regime, the resonator has an average phonon occupation which approaches zero, and displacement fluctuations are due to the quantum mechanical ground state energy of the resonator, which equals that of half a phonon. The root-mean-square value of the ground state displacement fluctuations is called the zero-point motion and is given by [3]:

$$u_{zpf} = \sqrt{\frac{h f_R}{2m_R(2\pi f_R)^2}} \quad (8)$$

The maximum power spectral density  $S_{uu}(f)$  due to the zero-point motion occurs at the resonance frequency and is related to  $u_{zpf}$  according to [3]:

$$S_{uu}^{zpf}(f_R) = u_{zpf}^2 \left( \frac{\pi f_R}{2Q} \right)^{-1} = \frac{hQ}{\pi m_R (2\pi f_R)^2} \quad (9)$$

where  $Q$  is the quality factor of the resonator. In order to measure the zero-point fluctuations, the measurement sensitivity of the detector should be better (lower) than  $S_{uu}^{zpf}(f_R)$ . The suspended carbon nanotubes in this paper each have a fundamental eigenmode with displacement in the direction of the back gate. Figure S3 shows a measurement of the mechanical response of the fundamental mode of one of the nanotubes to an applied driving force. From the response curve, we find a resonance frequency of 126 MHz and a quality factor  $Q = 3 \times 10^4$ . The mass of an 800 nm long single-walled carbon nanotube is approximately  $m_R = 5 \times 10^{-21}$  kg (and the corresponding spring constant is thus  $k = 3 \times 10^{-3}$  N/m). Using this lower bound for  $Q$  gives  $u_{zpf} = 3.6$  pm and  $\sqrt{S_{uu}^{zpf}(f_R)} = 45$  fm/ $\sqrt{\text{Hz}}$ . With the above responsivity, the zero-point fluctuations of a single suspended nanotube segment result in a flux noise in the SQUID of  $16 \mu\Phi_0/\sqrt{\text{Hz}}$ .

## S5 Estimates of coupling for a nanotube transmon qubit

The zero-phonon coupling rate  $g$  is given by the shift in the energy levels of the qubit in response to the zero-point fluctuations of the nanotube position [4, 5]. The zero point fluctuations of  $u_{zpf} = 3.6$  pm together with the responsivity of  $0.35 \text{ m}\Phi_0/\text{pm}$  gives a corresponding flux shift of  $\Phi_{ZPF} = 1.3 \text{ m}\Phi_0$ . In the transmon limit, where the charging energy is much smaller than the Josephson energy ( $E_C \ll E_J$ ), the energy splitting of the qubit is given by [6]:

$$E_{01} \approx \sqrt{8E_J E_C} \quad (10)$$

A small change in the qubit energy due to a change in the Josephson energy is then given by:

$$\delta E_{01} = \frac{E_{01}}{2} \frac{\delta E_J}{E_J} \quad (11)$$

We now need to estimate  $\delta E_J$  in response to the  $\Phi_{ZPF}$  above. Our SQUID shows a near complete suppression of the critical current as a function of flux, allowing us to estimate the change in  $E_J$  on the slope of the flux oscillation as

$$\frac{dE_J}{d\Phi} \approx \frac{E_J^{max}}{0.5\Phi_0} \quad (12)$$

The coupling rate  $g$ , given by the shift of the qubit energy in response to the zero point fluctuations of the nanotube position, can then be estimated as:

$$g = \delta E_{01}^{ZPF} \approx \frac{E_{01}}{2} \frac{\Phi_{ZPF}}{0.5\Phi_0} \quad (13)$$

Assuming  $E_{01}$  is designed to be 6 GHz, and using  $\Phi_{ZPF} = 1.3 \text{ m}\Phi_0$ , we estimate the coupling to be  $g = 7$  MHz.

## References

- [1] Hüttel, A. *et al.* Carbon nanotubes as ultrahigh quality factor mechanical resonators. *Nano Lett.* **9**, 2547–2552 (2009).
- [2] Sapmaz, S., Blanter, Y., Gurevich, L. & Van Der Zant, H. Carbon nanotubes as nanoelectromechanical systems. *Physical Review B* **67**, 235414 (2003).
- [3] Poot, M. & van der Zant, H. Mechanical systems in the quantum regime. *Phys. Rep.* **511**, 273–335 (2012). URL <http://www.sciencedirect.com/science/article/pii/S0370157311003644>.
- [4] LaHaye, M., Suh, J., Echternach, P., Schwab, K. & Roukes, M. Nanomechanical measurements of a superconducting qubit. *Nature* **459**, 960–964 (2009).
- [5] Chan, J. *et al.* Laser cooling of a nanomechanical oscillator into its quantum ground state. *Nature* **478**, 89–92 (2011).
- [6] Koch, J. *et al.* Charge-insensitive qubit design derived from the cooper pair box. *Phys. Rev. A* **76**, 042319 (2007).